CERAMIC/METAL NANOCOMPOSITES BY LYOPHILIZATION: PROCESSING AND HRTEM STUDY

C.F. Gutierrez-Gonzalez[a], S. Agouram[b], R. Torrecillas[a], J.S. Moya[c] and S. Lopez-Esteban[a]*

[a]Centro de Investigación en Nanomateriales y Nanotecnologia (CINN) [Consejo Superior de Investigaciones Cientificas (CSIC)-Universidad de Oviedo (UO)-Principado de Asturias (PA)]; Parque Tecnologico de Asturias, 33428 Llanera (Spain).
[b]SCSIE, Universidad de Valencia, P.O. Box 22085, 46071 Valencia, Spain.
[c]Instituto de Ciencia de Materiales de Madrid, Consejo Superior de Investigaciones Cientificas (ICMM-CSIC), Cantoblanco, 28049 Madrid (Spain).

Corresponding author. E-mail: s.lopez@cinn.es, Tel.: +34-985.98.00.58 (ext. 256). Fax: +34-985.26.55.74. Centro de Investigacion en Nanomateriales y Nanotecnologia (CINN). Consejo Superior de Investigaciones Cientificas (CSIC). Edificio ITMA, Parque Tecnologico de Asturias, 33428 Llanera, Asturias, Spain.

ABSTRACT

This work describes a wet-processing route based on spray-freezing and subsequent lyophilization designed to obtain nanostructured ceramic/metal powders. Starting from the ceramic powder and the corresponding metal salt, a water-based suspension is sprayed on liquid nitrogen. The frozen powders are subsequently freeze-dried, calcined and reduced. The material was analyzed using X-ray diffraction analysis at all stages. High Resolution Transmission Electron Microscopy studies showed a uniform distribution of metal nanoparticles on the ceramic grain surfaces, good interfaces and high crystallinity, with an average metal particle size in the nanometric range.

KEYWORDS: A. composites; A. nanostructures; B. freeze-drying; C. electron microscopy; D. microstructure.

1. Introduction

Due to their interesting properties and applications, nanostructured materials are nowadays the object of one of the most outstanding lines of research. Concerning ceramics, it is well known that the presence of a nanometric microstructure is responsible for the enhancement of different properties, such as mechanical [1,2], catalytic [3,4] optical [5,6], etc. Numerous techniques have been developed to produce nanoparticles, among which the ones that are increasing in popularity are vapour-phase synthesis (CVD [7,8], spray pyrolysis [9,10], laser pyrolysis [11,12]) or wet routes such as sol-gel [13,14].

This work is focused on ceramic-based nanocomposite powders formed by oxide ceramic matrices with well-dispersed metal and/or semiconductor nanoparticles, which are promising materials for structural and multifunctional applications [15-17]. A broad spectrum of synthesis techniques have been used with different ceramic/metal systems [15]. Unfortunately, use of nanosized powders involves dealing with the strong tendency of the nanoparticles to agglomerate [18]. In order to avoid this negative effect, using wet processing routes of colloidal suspensions followed by a fast drying method has become one of the most active research areas in ceramics. In this context, the interest of this work is to synthesize ceramic/metal nanocomposite powders using spray-freezing and, subsequently, lyophilization as drying method (also known as "freeze drying").

Spraying allows dividing the suspension into very small drops, which increases the speed of freezing when sprayed over liquid nitrogen. This avoids the segregation of components. Lyophilization consists of sublimating ice under vacuum and low temperature conditions. When the lyophilization is properly controlled, water separates from the solid phases through sublimation and eliminates the capillary forces causing the nanoparticles [19]

to agglomerate. Maintaining the suspension frozen throughout the drying process is the most obvious advantage of lyophilization over liquid-phase drying. In liquid-phase drying, the top layer of liquid evaporates quickly causing a concentration of the particles at the surface. This creates an impermeable skin inhibiting the drying of the rest of the suspension. Such effects are avoided by lyophilization which, in addition, is a drying procedure commonly used by industries.

In this context, the aim of this **work** is to explain the potential of the lyophilization technique and to highlight specific features of its use in the preparation of composite materials consisting of a ceramic matrix with homogeneous and well dispersed metal nanoparticles as a second phase.

2. Experimental

2.1. Starting materials

The following commercially available powders have been used as raw materials: (1) Tetragonal zirconia polycrystals (3Y-TZP, 3 mol% Y_2O_3; *TZ-3YE, Tosoh Corp*.), with an average particle size of d_{50}=0.26±0.05 microns; (2) nickel (II) nitrate hexahydrate (*Merck*, Germany, 99.0% purity, $Ni(NO_3)_2 \cdot 6H_2O$).

2.2. Synthesis

Nickel nitrate salt powders were dispersed in distilled water by ultrasonic agitation in a suitable volume to achieve total dissolution. The ceramic powder was added in order to obtain zirconia/Ni composites with a metal content of 1 vol% Ni, 2.5 vol% Ni and 3.5 vol% Ni; the corresponding samples have been denoted as LF1, LF2.5 and LF3.5, respectively.

The suspensions were milled for 24 h with zirconia balls in order to get an homogeneous slurry (Figure 1A). As the materials were prepared in distilled water in order to be subsequently lyophilized, the stability of the dispersions was specifically studied in aqueous media. Several suspensions with different wt. % solid content were prepared with different additions of an alkali-free organic polyelectrolyte as surfactant for different relative proportions of metal. The sedimentation behaviour of the water-based slurries was studied at room temperature in glass test tubes for times up to 24 h. Finally, the best homogeneity was reached by the suspensions with 70 wt.% solids and 1 wt % surfactant. TEM studies made on selected samples corroborate these results.

The mixture was sprayed over liquid nitrogen (Figure 1B) with an airbrush gun *(Iwata Custom Micron SB* airbrush, *Iwata Medea, Inc.*, Portland, OR, USA) equipped with a 0.18 mm diameter nozzle. The frozen suspension was subsequently freeze-dried (Figure 1C) for 48 hours in a lyophilizer (*Cryodos-50, IMA-TELSTAR, S.L.*, Barcelona, Spain) until completely dried. The temperature of the cold finger in this equipment is continuously set at -50±2ºC. The freeze dryer shelf temperature and the chamber pressure during the entire process were +20±2ºC and 0.06±0.01 mbar, respectively. These conditions, according to the Phase Diagram of water, correspond to water vapor.

The resulting powder was calcined at 600°C for 2 hours in air to obtain ZrO_2/NiO powders [20,21]. Finally, the metal oxide was reduced to metallic nickel in a 90%Ar/10%H_2 atmosphere at 500°C for 2 hours, obtaining a zirconia powder with metal nanoparticles adhered to the surface of the ceramic grains (zirconia/nNi).

2.3. Characterization

X- ray diffraction analysis of the nanopowders at different stages of the processing route was used for phase identification using Cu K_α radiation (*XRD Bruker AXS D8 ADVANCE*, with a *SolX* energy-dispersive detector).

Further characterization of the samples was performed by Transmission Electron Microscopy (TEM), high resolution TEM (HRTEM) and Energy Dispersive X-Ray Spectroscopy (EDX-mapping) by using a Field Emission Gun (FEG) *TECNAI G2 F20* microscope operated at 200 kV. In order to prepare the TEM samples, the ZrO_2/Ni powder specimens were treated by sonicating in absolute ethanol for several minutes, and a few drops of the resulting suspension were deposited onto a holey-carbon film supported on a copper grid, which was subsequently dried. The samples were also used to determine the elemental content by EDX.

3. Results and discussion

3.1. X-Ray Diffraction

Figure 2 shows the X-ray diffractograms of sample LF3.5 in the 2θ range 10º-70º obtained at different stages of the processing route. The results confirm that products at the first stage consisted only of zirconia and nickel nitrate with no presence of any other phases (Figure 2a). After calcination, the nickel nitrate was oxidized into NiO (Figure 2b). No presence of either nickel nitrate or nickel oxide was detected in the final powder, which consisted only of zirconia/nNi (Figure 2c). The same results were obtained for the other two compositions (LF1 and LF2.5).

3.2. Transmission Electron Microscopy (TEM)

A representative TEM-EDX spectrum is shown in Figure 3. In the spectrum, it is possible to discern clearly the presence of Zr, O and Ni peaks. The C and Cu peaks are due to the TEM holey carbon-Cu grid. The quantitative EDX results are reported in Table 1.

Figure 4 shows the typical TEM micrographs and EDX-mapping of distributions of Ni nanoparticles and zirconia matrix for the sample with 2.5 vol. % Ni. These micrographs reveal that metal particles obtained are in the nanometer range and appear homogeneously and well dispersed on the zirconia surface.

More than 100 particles from all over the sample were measured to determine the Ni particle size distribution for each composition. As indicated in Figure 5A, the mean size of the nickel nanoparticles increases with the Ni content. In the sample with 1 vol. % Ni (Figure 5B) the particle size distribution is narrow and centered around 16-19 nm. Samples prepared with 2.5 and 3.5 vol.% Ni present a broader distribution, between 20-30 nm and 22-42 nm (Figures 5C and 5D, respectively). In all cases, the nanoparticle average size is lower than 35 nm.

3.3 HRTEM characterization

3.3.1. Ceramic submicron particles

A closer view of the nanostructure of the ZrO_2 matrix after deposition of the Ni nanoparticles with different content of Ni was carried out by HRTEM. Figure 6A shows the clear lattice spacing indicating that the nanoparticles are highly crystallized with an interplanar spacing of 2.62 Å, corresponding to the (002) planes of ZrO_2; the spacing of 2.55 Å between adjacent lattice planes corresponds to the (110) planes of ZrO_2; another interplanar distance of

1.82 Å corresponds to (112) planes of ZrO_2. *Fast Fourier Transform* (FFT) pattern of the selected zone in Figure 6B clearly illustrates the monocrystalline structure which could be indexed by a tetragonal phase, space group P42/nmc (137) in [-110] zone axis ZA (JCPDS: 83-113). Similar features were observed for other samples with different contents of Ni.

3.3.2. Nickel nanoparticles

High resolution TEM image and the FFT pattern of the selected zone are presented in Figure 7. The Ni nanoparticles appear as discrete, uniform and crystalline with a size around 20 nm. The Ni nanoparticles show a well defined lattice spacing of 2.05 Å, corresponding to the (111) planes of face-centered cubic phase of Ni, space group *Fm3m (225)* (JCPDS: 4-850). In all cases, these powders present an accurate composition, homogeneity and a good dispersion of metal. Likewise, the Ni nanoparticles are firmly attached to the zirconia particles, avoiding their coalescence.

3.3.3. Ceramic/metal interface

Further structural characterization of the powders was carried out using HRTEM to study the nature of the interface between the Ni nanoparticles and the zirconia matrix. Figure 8 illustrates a representative micrograph. The interface is ordered, very neat, showing that the Ni nanoparticles have grown epitaxially on the surface of zirconia. This effect has already been observed in samples obtained by a different drying method [22]. The origin of such a good degree of epitaxy in 3Y–TZP/Ni nanocomposites can be due to two reasons: i) a very good lattice matching between ZrO_2 and nickel and ii) the “evaporation-condensation” grain growth mechanism present in metallic nanoparticles. The combined effect of these factors produces a real epitaxial growth of Ni crystals on ZrO_2 submicron grains. This feature is positive as, theoretically, it may lead to excellent mechanical properties in the corresponding sintered

materials. Therefore, the future work will be focused on investigating different sintering routes and, subsequently, the features of the dense materials.

4. Conclusions

This work demonstrates that combining spray-freezing with lyophilization is a feasible technique for preparing ceramic/metal nanostructured powders. In this work, three different metal contents in the zirconia/nickel system have been studied, showing in all cases that the resulting powders present accurate composition, homogeneity and good dispersion of metal. The metal nanoparticle size distribution is centred between 17 nm and 35 nm, depending on the metal concentration. Both phases, ceramic and metal, present a good degree of crystallinity. The metal nanoparticles have grown epitaxially on the ceramic surface giving rise to good interfaces, which is crucial to obtain excellent mechanical properties in the corresponding sintered materials.

Acknowledgements

This work was supported by the Spanish Ministry of Science and Innovation (MICINN) under the project MAT2009-14542-C02. C.F. Gutierrez-Gonzalez acknowledges CSIC and ESF for the concession of a JAE-Doc 2009 grant. S. Agouram thanks the Spanish Ministry of Science and European Social Fund for financial support. The authors thank the contribution of M. Anel for the Scheme in Figure 1.

REFERENCES

[1] S. Hao, H. Wang, Adv. Mater. Res. 168-170 (2011) 1846-1849.

[2] M. Yi, C. Xu, J. Zhang, Z. Jiang, Adv. Eng. Mater. 154-155 (2011) 1356-1360.

[3] A. Folli, I. Pochard, A. Nonat, U.H. Jakobsen, A.M. Shepherd, D.E. Macphee, J. Am. Ceram. Soc. 93 (2010) 3360-3369.

[4] D. Thiele, Mater. Chem. and Phys. 124 (2010) 529-534.

[5] R.M. Krsmanović, Z. Antić, M.G. Nikolić, M. Mitrić, M.D. Dramićanin, Ceram. Int. 37 (2011) 525-531.

[6] Y. Zorenko, T. Voznyak, V. Gorbenko, E. Zych, S. Nizankovski, A. Dan'Ko, V. Puzikov, J. Lumin. 131 (2011) 17-21.

[7] J.H. Kim, S.K. Lee, O.M. Kwon, D.S. Lim, J. Nanosci. Nanotechno. 9 (2009) 4121-4127.

[8] K. Kubota, Int. J. Jpn. Soc. Precis. Eng. 76 (2010) 1336-1339.

[9] H.Y. Koo, J.H. Kim, Y.N. Ko, Y.C. Kang, V.D. Nguyen, D. Byun, B.K. Kim, J. Ceram. Soc. Jpn. 118 (2010) 613-616.

[10] M.I. Martín, L.S. Gómez, O. Milosevic, M.E. Rabanal, Ceram. Int. 36 (2010) 767-772.

[11] R. Dez, F. Ténégal, C. Reynaud, M. Mayne, X. Armand, N. Herlin-Boime, J. Eur. Ceram. Soc. 22 (2002) 2969-2979.

[12] A. Müller, N. Herlin-Boime, F. Ténégal, X. Armand, F. Berger, A.M. Flank, R. Dez, K. Müller, J. Bill, F. Aldinger, J. Eur. Ceram. Soc. 23 (2003) 37-46.

[13] M. Miranda, A. Fernández, E. Saiz, A.P. Tomsia, R. Torrecillas, Int. J. Mater. Res. 101 (2010) 117-121.

[14] R. Torrecillas, M. Díaz, F. Barba, M. Miranda, F. Guitián, J.S. Moya, J. Nanomater. (2009) art nº 498505.

[15] J.S. Moya, S. Lopez-Esteban, C. Pecharroman, Prog. Mater. Sci. 52 (2007) 1017-1090.

[16] K. Niihara, J. Ceram. Soc. Jpn. 99 (1991) 974 - 982.

[17] S. Lopez-Esteban, C.F. Gutierrez-Gonzalez, G. Mata-Osoro, C. Pecharroman, L.A. Diaz, R. Torrecillas, J.S. Moya, Scripta Mater. 63 (2010) 219-222.

[18] J. Li, Y.Q. Lin, B.G. Zhao, J. Nanopart. Res. 4 (2002) 345-349.

[19] B.E. Novich, C.A. Sundback, R.W. Adams, Quickset Injection Molding of High-Performance Ceramics, M. J. Cima. American Ceramic Society, Westerville, OH, 1992.

[20] F. Esteban-Betegon, S. Lopez-Esteban, J. Requena, C. Pecharroman and J.S. Moya. J. Am. Ceram. Soc., 89 [1] (2006) 144–150.

[21] S. Lopez-Esteban, M. Diaz, J.S. Moya. Comp. Sci. Technol. 67 (2007) 2303–2310.

[22] C. Pecharroman, J.I. Beltran, F. Esteban-Betegon, S. Lopez-Esteban, J.F. Bartolome, M.C. Munoz, J.S. Moya, Z. Metallkd. 96 (2005) 507-514.

TABLES

% at.	LF1	LF2.5	LF3.5
O	69.4	69.2	65.8
Zr	29.0	28.2	31
Ni	1.6	2.6	3.2

Table 1: Quantitative EDX analysis the samples with different content of Ni (% at.).

FIGURE CAPTIONS

Figure 1. Scheme of the processing route of the nanocomposite powders. The nickel nitrate salt powders were dispersed in distilled water with the ceramic powder and milled for 24 h with zirconia balls in order to get an homogeneous slurry (A). The mixture was sprayed with an airbrush gun (0.18 mm diameter nozzle) on liquid nitrogen (B) and subsequently freeze-dried (C).

Figure 2. X-ray diffractograms corresponding to the nanopowder with LF3.5 obtained at different stages of the processing route: (a) Lyophilized 3Y-TZP/$Ni(NO_3)_2 \cdot 6H_2O$, (b) calcined 3Y-TZP/NiO, (c) reduced 3Y-TZP/Ni.

Figure 3. TEM-EDX spectrum of LF3.5 sample.

Figure 4. TEM micrograph of the 3Y-TZP/Ni powder with 2.5 vol% Ni (A). EDX mapping showing in green the Ni nanoparticles (B).

Figure 5: Histograms and evolution of average size of Ni nanoparticles as a function of the initial Ni content.

Figure 6. HRTEM micrograph corresponding to LF2.5 (A) and FFT pattern of the selected area (B).

Figure 7. (A) HRTEM micrograph corresponding to LF2.5. (B) Detail of Ni nanoparticle and the corresponding index assignment. (C) FFT pattern of the Ni nanoparticle.

Figure 8. HRTEM micrograph of Ni nanoparticle epitaxially grown on the surface of zirconia submicron particle. The interface between both particles presents an excellent matching of atomic planes.

*Graphical Abstract

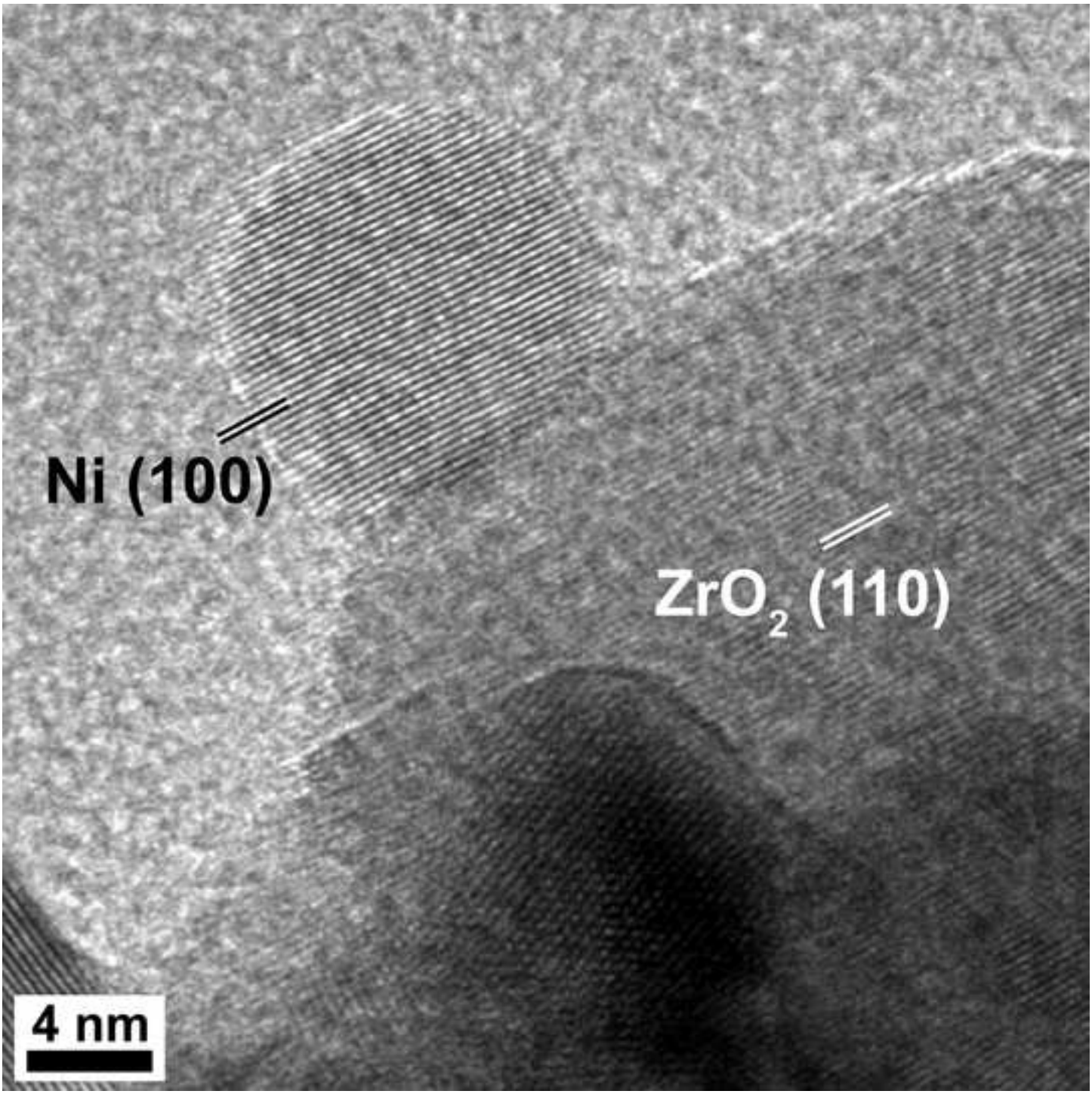

Figure 1

Click here to download high resolution image

Figure 2

Click here to download high resolution image

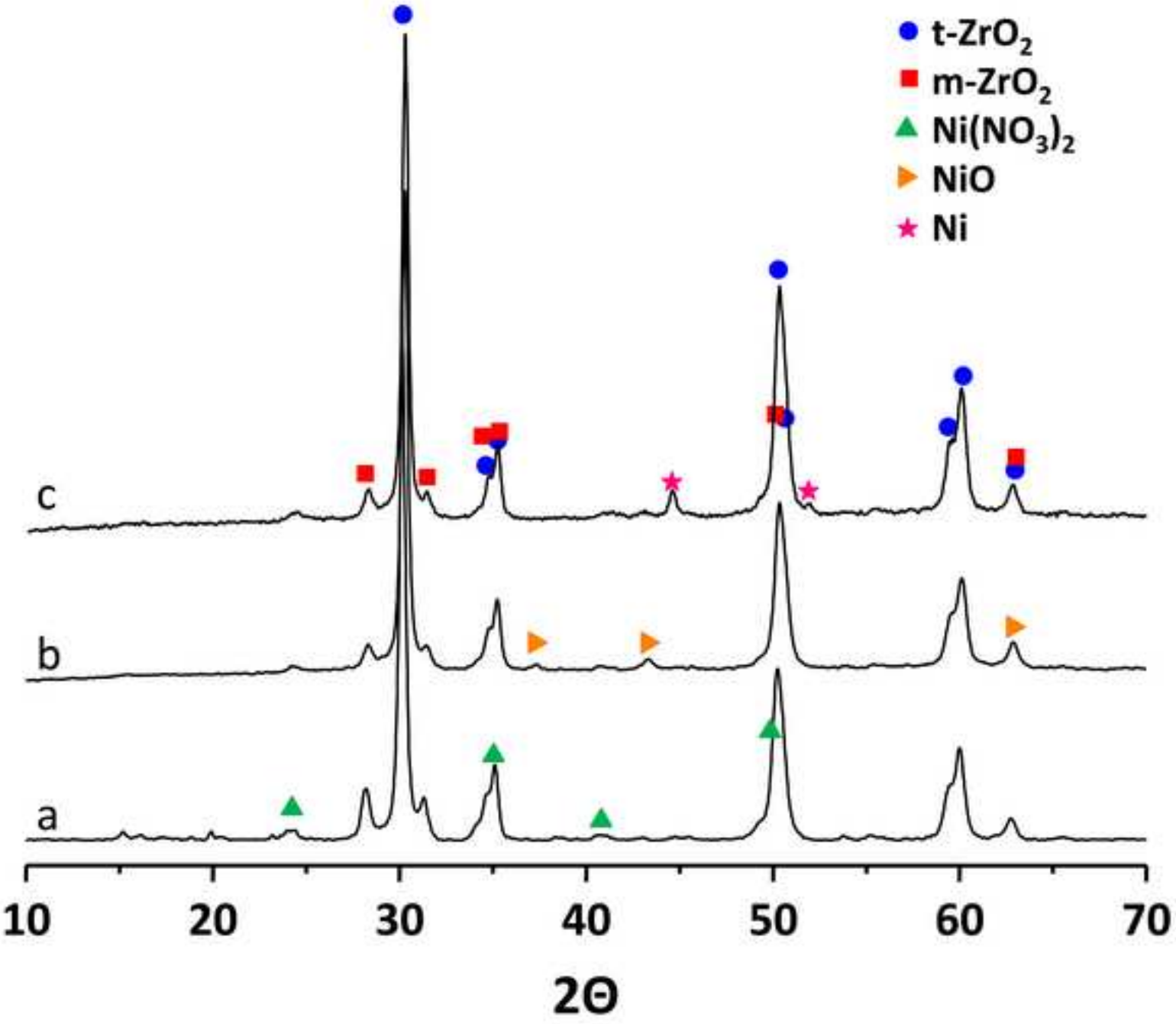

Figure 3

Click here to download high resolution image

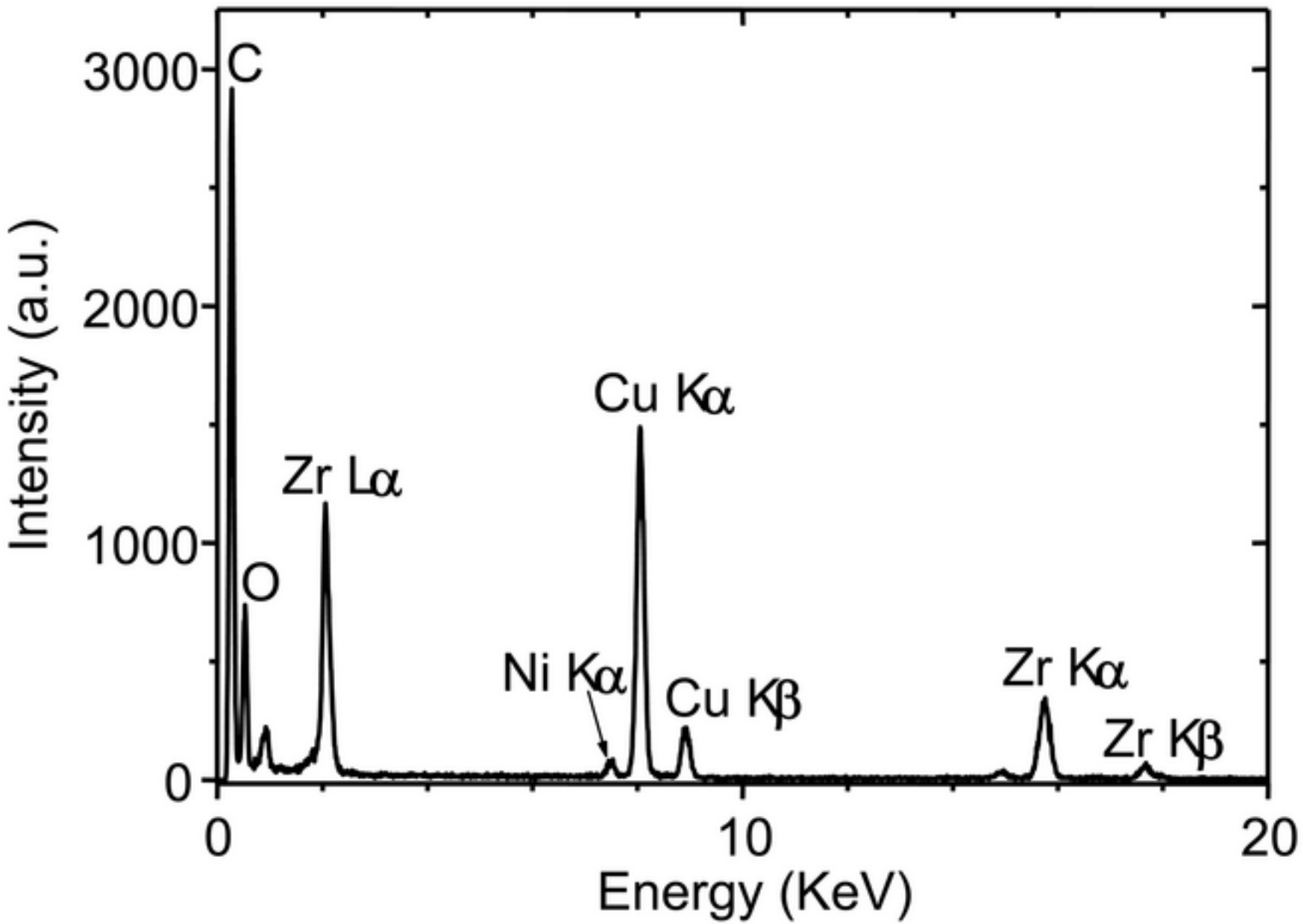

Figure 4

Click here to download high resolution image

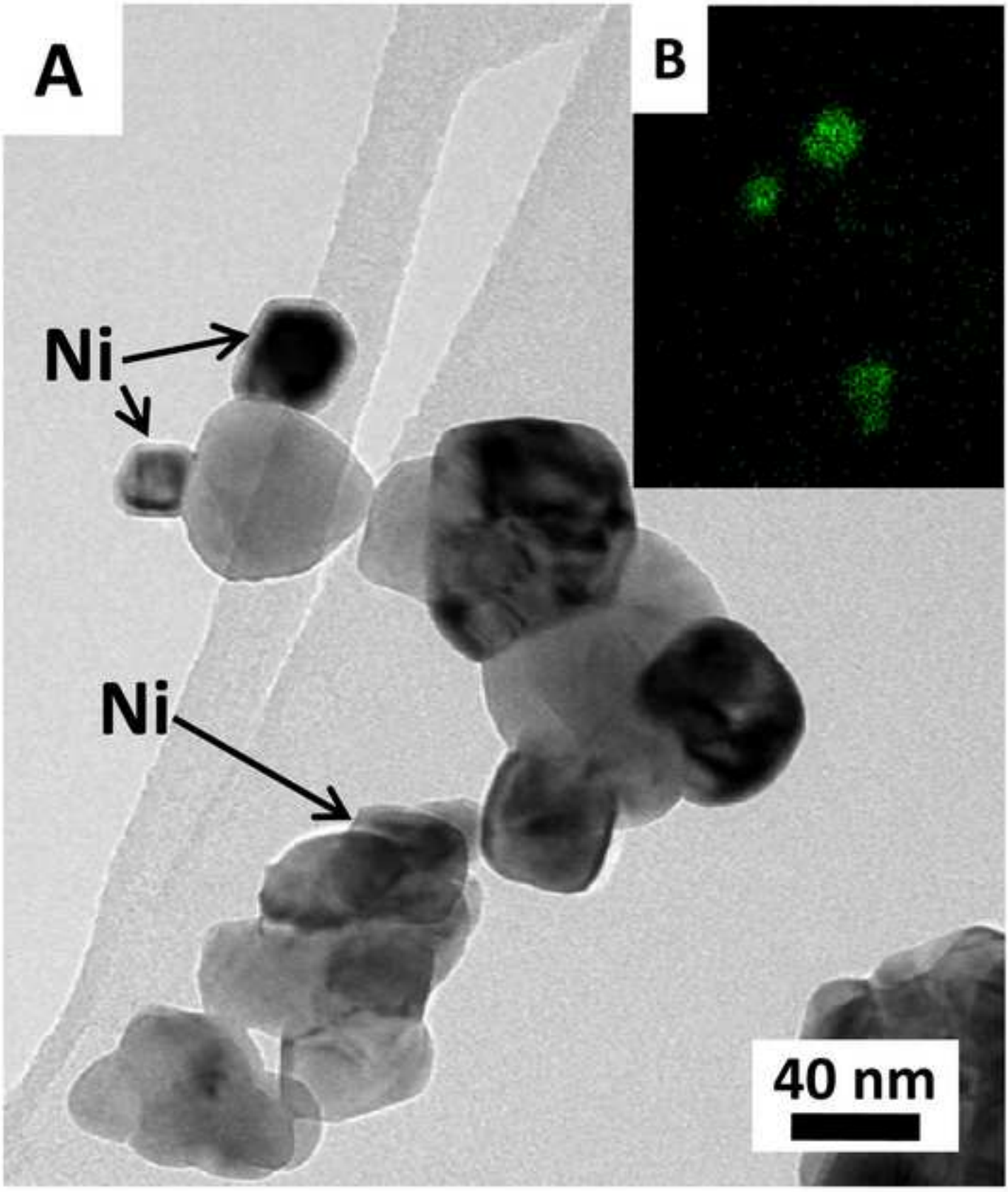

Figure 5

Click here to download high resolution image

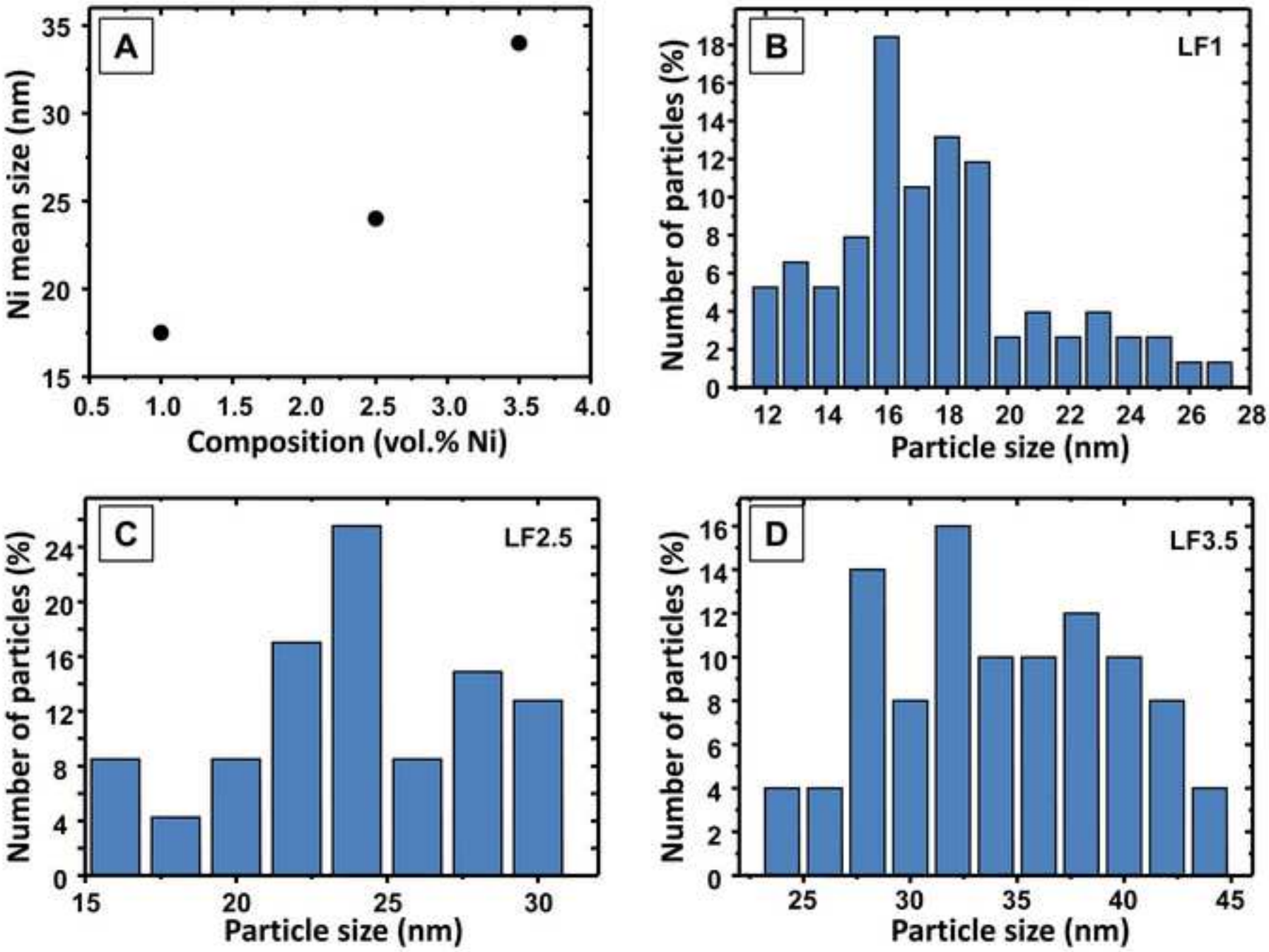

Figure 6

Click here to download high resolution image

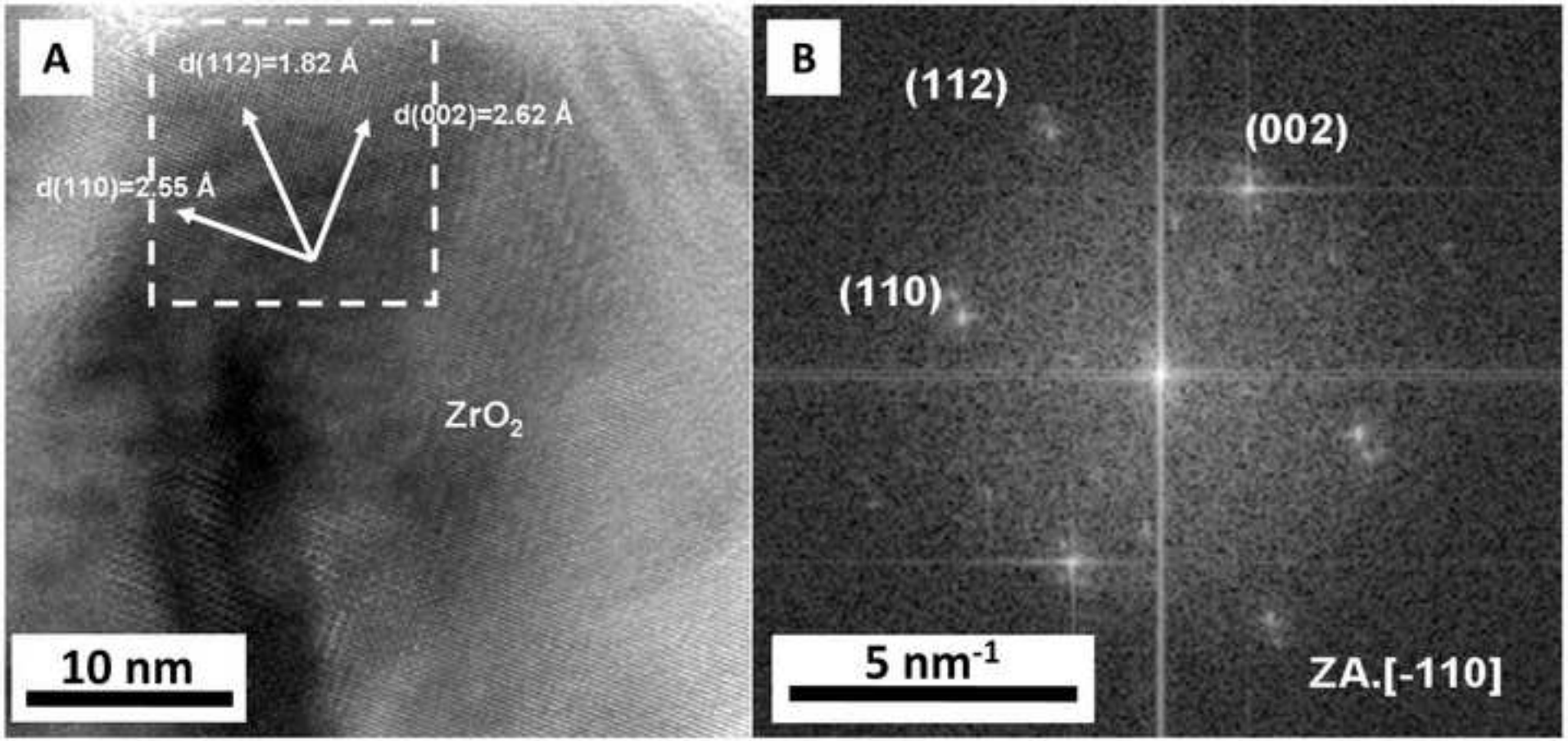

Figure 7

Click here to download high resolution image

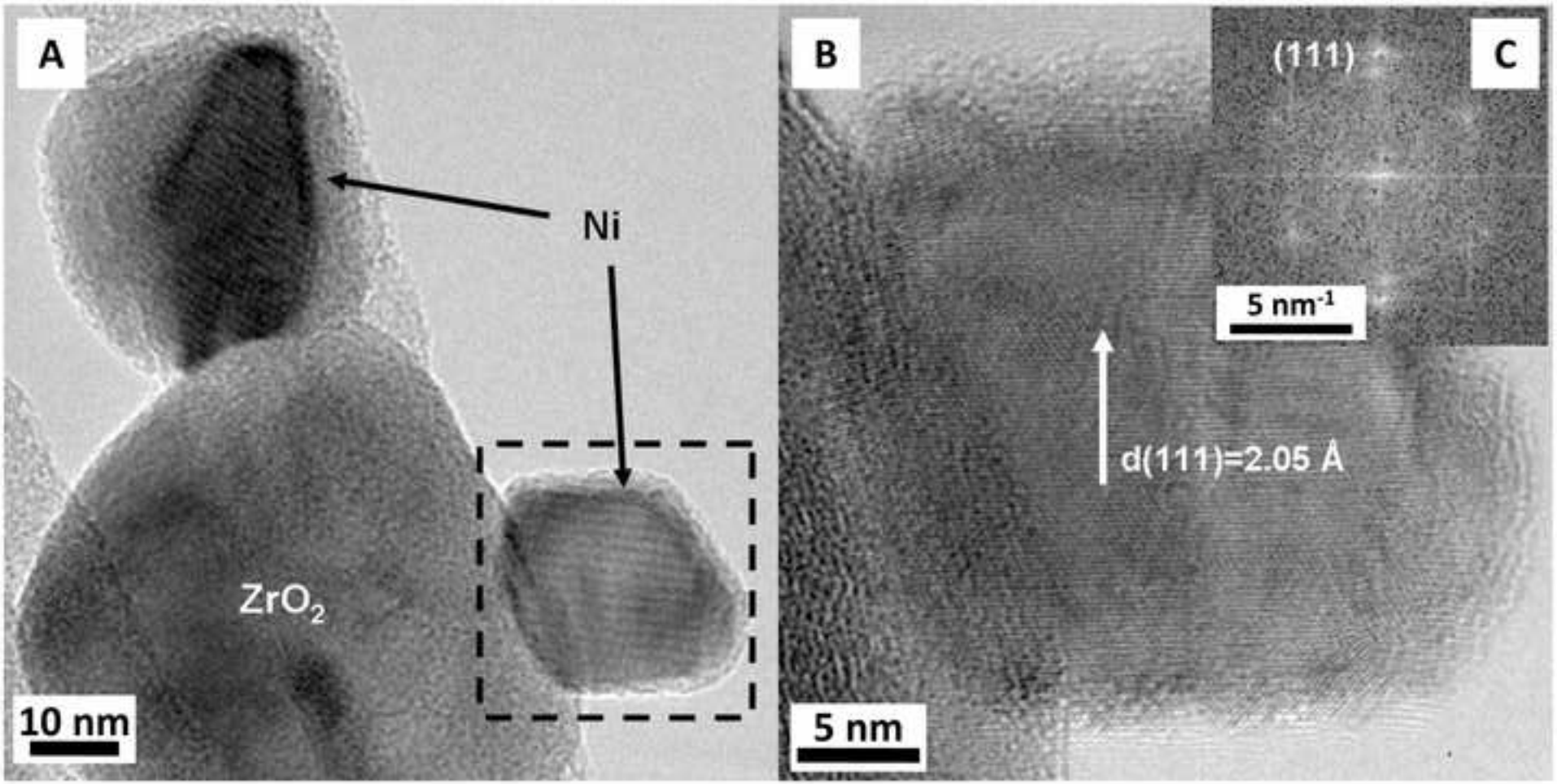

Figure 8

Click here to download high resolution image

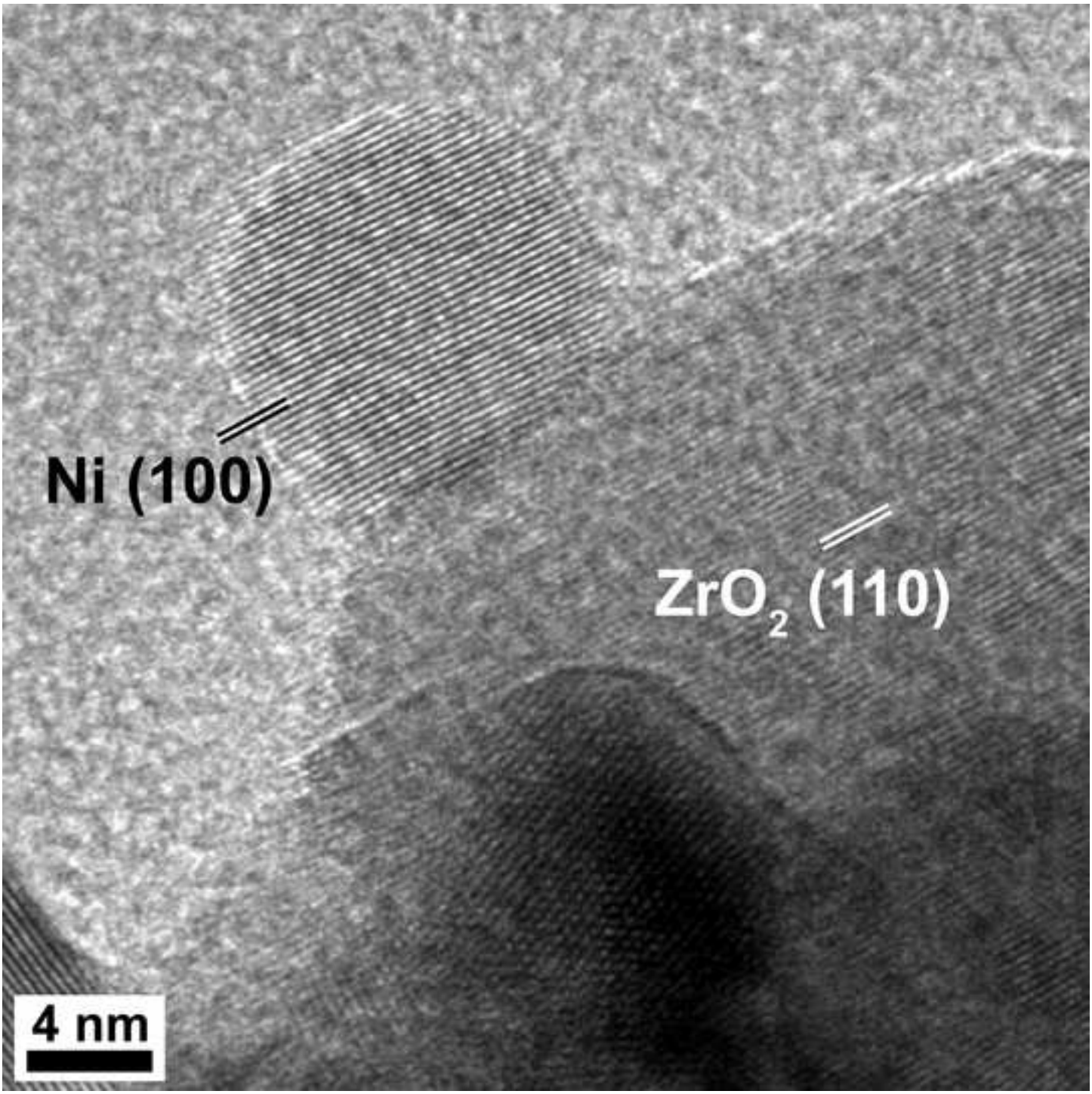

TABLES

% at.	LF1	LF2.5	LF3.5
O	69.4	69.2	65.8
Zr	29.0	28.2	31
Ni	1.6	2.6	3.2

Table 1: Quantitative EDX analysis the samples with different content of Ni (% at.).